Coupling between fast and slow oscillator circuits in *Cancer borealis* is temperature compensated

Powell, D.J.* dpowell@brandeis.edu https://orcid.org/0000-0002-9210-2201

Haddad, S.A.*[1] sara.haddad@mls.uzh.ch https://orcid.org/0000-0003-0807-0823

Gorur-Shandilya, S.* srinivasgs@brandeis.edu https://orcid.org/0000-0002-7429-457X

Marder, E. marder@brandeis.edu https://orcid.org/0000-0001-9632-5448

Biology Department and Volen Center, Brandeis University, Waltham, MA 02454

Corresponding author: Eve Marder marder@brandeis.edu

*Authors contributed equally to this work

[1] Present address:
Department of Molecular Life Sciences
University of Zürich, Irchel
Winterthurerstrasse 190
CH-8057 Zürich, Switzerland

Key Words: pyloric rhythm, gastric mill rhythm, stomatogastric ganglion, central pattern generator, integer coupling

Abbreviated title: Stable temperature coupling of fast and slow oscillators

Contributions: project conception: SAH, DJP, EM; data collection: SAH, DJP; data analysis: SGS; Figure creation: SGS, DJP; manuscript writing and editing: DJP SAH SGS EM

Acknowledgments: We thank Dr. Michael P Nusbaum for insights relevant to the operation of the gastric mill circuit.

Research supported by: 5T32-NS007292 (SGS); R35-NS097343 (EM)

Abstract

Coupled oscillatory circuits are ubiquitous in nervous systems. Given that most biological processes are temperature sensitive, it is remarkable that the neuronal circuits of poikilothermic animals can maintain coupling across a wide range of temperatures. Within the stomatogastric ganglion (STG) of the crab *Cancer borealis*, the fast pyloric rhythm (~1Hz) and the slow gastric mill rhythm (~0.1Hz) are precisely coordinated at ~11°C such that there are an integer number of pyloric cycles per gastric mill cycle (integer coupling). Upon increasing temperature from 7-23°C, both oscillators showed similar temperature-dependent increases in cycle frequency, and integer coupling between the circuits was conserved. Thus, although both rhythms show temperature dependent changes in rhythm frequency, the processes that couple these circuits maintain their coordination over a wide range of temperature. Such robustness to temperature changes could be part of a toolbox of processes that enables neural circuits to maintain function despite global perturbations.

Introduction

Coupled oscillators are common in nervous systems. Although oscillatory circuits may have distinct frequencies and duty cycles, coordination between them is often necessary for proper function (Nadim et al., 1998; Bartos et al., 1999; Colgin, 2011; Gordon, 2011; Jacobson et al., 2013; Rojas-Líbano et al., 2014; Harris and Gordon, 2015; Karalis et al., 2016; Tamura et al., 2017). For example, theta frequency circuits coupled to those in the gamma range are thought to drive both sensory and behavioral processing (Lisman and Buzsáki, 2008; Fujisawa and Buzsaki, 2011; Gordon, 2011; Lisman and Jensen, 2013). Memory formation may rely on the phase coupling of discrete populations of neurons with distinct frequency bands in the hippocampus (Tass et al., 1998; Lisman, 2005; Montgomery and Buzsaki, 2007; Scheffer-Teixeira and Tort, 2016; Zheng et al., 2016). Possible consequences of uncoupling or improper coupling of oscillatory circuits include disease states and circuit malfunction (Moran and Hong, 2011; Kirihara et al., 2012; de Hemptinne et al., 2013; Bahramisharif et al., 2016; Salimpour and Anderson, 2019). The coordination of oscillatory circuits, often with distinct temporal features, is therefore key to circuit function and information processing. Because fluctuations in a circuit's environment can impact function (Fonseca and Correia, 2007; Tang et al., 2010; Haddad and Marder, 2018; Haley et al., 2018; Kushinsky et al., 2019; He et al., 2020), how robust is this coordination to externally or internally generated perturbations?

The stomatogastric ganglion (STG) of the Jonah crab (*Cancer borealis*) contains two well characterized coupled oscillatory circuits with known connectivity that generate distinct rhythms with different cycle periods (Coleman et al., 1995; Nadim et

al., 1998; Marder and Bucher, 2007). The pyloric rhythm (~1 Hz) is driven by a three neuron bursting pacemaker kernel composed of the single Anterior Burster (AB) neuron and two Pyloric Dilator (PD) neurons (Nadim et al., 1998; Marder and Bucher, 2007). The gastric mill rhythm (~0.1 Hz) is produced by activating a half-center oscillator (reciprocal inhibition that produces alternating bursts of activity) between the Lateral Gastric (LG) motor neuron and Interneuron 1 (Int1), and it depends on a complex set of mechanisms including electrical junctions, and modulatory input (Coleman and Nusbaum, 1994; Coleman et al., 1995; Bartos and Nusbaum, 1997; Nadim et al., 1998; Bartos et al., 1999; Marder and Bucher, 2007; Stein et al., 2007). Although the pyloric and gastric mill oscillators independently produce distinct rhythms (Bartos et al., 1999), the core generator neurons (AB and LG) are integer coupled to each other and influence one another (Coleman and Nusbaum, 1994; Marder et al., 1998; Nadim et al., 1998). These circuits face a challenge as they must cope with extrinsic perturbations such as temperature fluctuations and other environmental factors that the crabs experience (Marder et al., 2015).

In the New England Atlantic Ocean, where *C. borealis* is found, intertidal temperatures normally range from 8-24°C during the summer and 3-18°C in the winter (Stehlik et al., 1991). Because temperature affects most biological processes differently, it poses an interesting challenge for the nervous systems of poikilothermic animals that experience substantial temperature changes (Hazel and Prosser, 1974; Zečević and Levitan, 1980; Prosser and Nelson, 1981; Burrows, 1989; Foster and Robertson, 1992; Xu and Robertson, 1994; Xu and Meldrum Robertson, 1996; Franz and Ronacher, 2002; Garrity et al., 2010; Marder et al., 2015). For example, the rate change across 10°C

(Q_{10}s) of ion channels can range from ~2 – 20 (Zečević et al., 1985; Klockner et al., 1990; Moran et al., 2004; Cao and Oertel, 2005; Fohlmeister et al., 2010; Tang et al., 2010; Kang et al., 2012; Robertson and Money, 2012; Yang and Zheng, 2014). Although the phase relationships between different pyloric neurons are stable between 7 and 23°C (Tang et al., 2010; Haddad and Marder, 2018), little is known about temperature compensation in the gastric mill oscillator (Stadele et al., 2015) or how temperature affects coupling between the pyloric and gastric mill rhythms.

A key feature of temperature compensation in the pyloric circuit is that the pacemaker kernel of the pyloric rhythm maintains constant duty cycle across a range of temperatures (Tang et al., 2010; Rinberg et al., 2013), and this facilitates temperature compensation of neuron phase relationships in the rest of the circuit. Because these two rhythm generators arise from different processes, it was not clear that the gastric mill rhythm would be phase compensated as a function of temperature, and whether the relationships between the two rhythms, such as integer coupling, would be maintained as temperature varies.

Results

Two rhythmic oscillators driven by different processes

There are two major rhythms produced by neurons in the STG. The pyloric rhythm is constitutively active, with a characteristic period of about 1 sec. The gastric mill rhythm can be evoked by stimulating projection neurons found within the commissural ganglia (CoGs), and has a characteristic period of 6-10 sec (Beenhakker et al., 2004). The modulatory commissural neuron 1 (MCN1) and commissural projection neuron 2 (CPN2) (**Fig. 1a**) evoke a gastric mill rhythm when stimulated or are spontaneously active (**Methods**) (Beenhakker et al., 2004).

The activity of both circuits can be monitored by extracellular recordings from the motor nerves exiting the STG. The gastric mill rhythm can be seen in the lateral gastric nerve (*lgn*), dorsal gastric nerve (*dgn*), and medial ventricular nerve (*mvn*) recordings in **Fig. 1b**. These recordings show alternating bursts of activity in the LG and Dorsal Gastric (DG) neurons, with the Gastric Mill (GM) neurons firing at the end of the LG burst. The VD (Ventricular Dilator) and IC (Inferior Cardiac) neurons, seen on the *mvn* show an envelope of activity alternating with the LG neuron, but also fire in time with the faster pyloric rhythm seen on the lateral ventricular nerve (*lvn*) and pyloric dilator nerve (*pdn*) (**Fig. 1b**). Because the AB and PD neurons are strongly electrically coupled, the cycle period of the pyloric pacemaker can be monitored using the *pdn* (**Fig. 1b**), which contains only PD action potentials. Similarly, the LG neuron indicates gastric mill rhythm cycle period (**Fig. 1b**).

Figure 1c is a connectivity diagram of neurons in the STG and shows how MCN1 and CPN2 activate the gastric mill neurons. While CPN2 drives the gastric mill circuit

132 via electrical synapses onto key motor neurons (LG and GM), MCN1 excites all neurons
133 in the STG, including the pyloric pacemaker and gastric mill half-center neurons (LG
134 and Int1) (**Fig. 1d**). Both pattern generating circuits provide feedback to these
135 projection neurons (Norris et al., 1994; Blitz and Nusbaum, 2008, 2012; Blitz, 2017).
136 The interactions between CPN2, MCN1, and LG shape the timing of the gastric mill
137 rhythm along with rhythmic inhibition of Int1 by AB that allows LG to be rhythmically
138 released from inhibition and burst (Coleman and Nusbaum, 1994; Coleman et al., 1995).
139 The cartoon voltage traces (**Fig. 1d**) demonstrate integer coupling between the pyloric
140 and gastric mill circuits, where rhythmic AB-inhibition of Int1 results in LG
141 disinhibition and firing following the peak of Int1 inhibition (Nadim et al., 1998; Bartos
142 et al., 1999) .

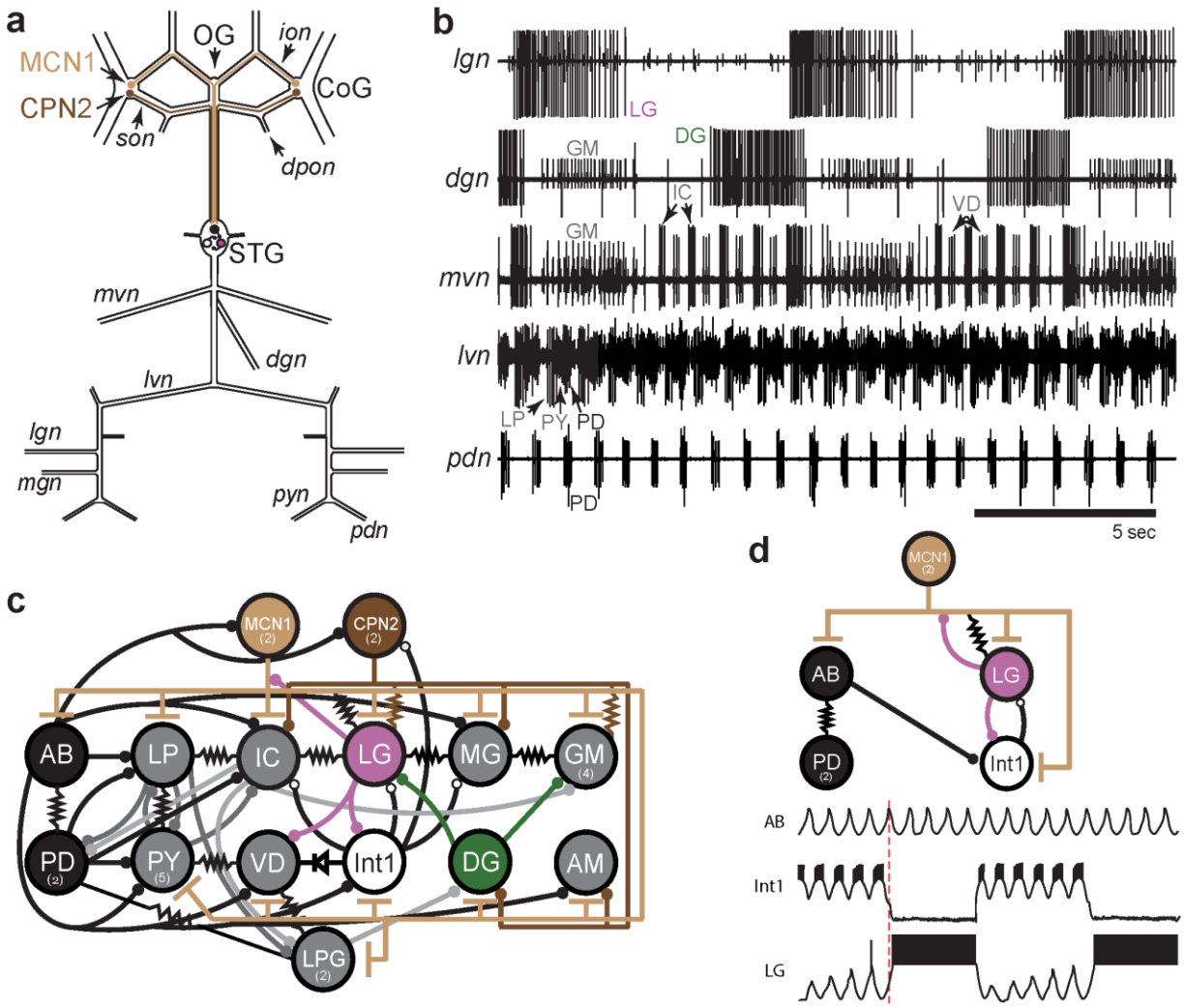

Figure 1. STG rhythmic motor patterns. (**a**) Schematic of the STNS showing the locations of salient ganglia, nerves, and projection neurons. Individual STG neurons are unambiguously identified on the basis of the motor nerves by which they project to specific stomach muscles. (**b**) Extracellular nerve recordings of both the gastric mill (*lgn*, *dgn*, *mvn*) and pyloric (*lvn*, *pdn*) rhythms. The gastric mill rhythm is seen as the alternating bursts of activity in the LG and DG neurons. The GM neurons are active late in the LG neuron burst. The IC and VD neurons are active in alternation with LG, but also show activity in time with the pyloric rhythm (*lvn)*, with the PD neurons shown obn the *pdn*. (**c**) Wiring diagram of the gastric mill, pyloric, and gastropyloric neurons and the input they receive from MCN1 (tan) and CPN2 (brown). LG (pink) and DG (olive) are both gastric mill neurons and AB-PD (black) are pyloric neurons. Colors used for these neurons are consistent in all figures. The resistor symbols denote electrical synapses; chemical inhibitory synapses are shown as filled circles, and the T bars indicate chemical excitatory/modulatory synapses from CPN2 and MCN1. (**d**) (Top) Simplified wiring diagram of MCN1 excitation of both pattern generating circuits and AB inhibition of Int1 (white). (Bottom) Cartoon voltage traces of AB, Int1, and LG as they would appear during a gastric mill rhythm showing the relative burst timing

between these neurons. As a consequence of a slow excitation from MCN1 to LG, the envelope of the disinhibition of the LG from Int1 increases slowly over several cycles, eventually resulting in LG crossing threshold and bursting in time with the AB neuron. Note that the slight delays between the peak of AB depolarization, the trough of Int1 inhibition from AB, and the subsequent burst of LG as marked by the dashed line.

Spontaneous gastric mill rhythms span a physiological range of temperatures

While the circuit controlling the pyloric rhythm is temperature robust across a temperature range from 7°C – 25°C (Tang et al., 2010; Tang et al., 2012; Rinberg et al., 2013; Soofi et al., 2014; Haddad and Marder, 2018), it remains unclear if the gastric mill circuit could also operate across this same range (Stadele et al., 2015). We inspected a dataset of extracellular recordings of *dgn* and *lgn* during temperature ramps (Haddad and Marder, 2018) and found spontaneous gastric mill activity at temperatures between 11°C and 30°C.

Figure 2a shows bursts of LG (*lgn*) and DG (*dgn*) neurons from a single preparation showing spontaneous gastric mill activity at these temperatures. While these recordings show relatively regular gastric mill rhythms at lower temperatures, they were less regular at higher temperatures. **Figure 2b** shows example raster plots of the LG neuron for two preparations with spontaneous gastric mill rhythms. Color indicates the temperature at which that rhythm was observed and can be seen in the raster plots from two preparations across a range of temperatures. Preparation 1 intermittently displayed characteristic gastric mill rhythms at both high and low temperatures, but was much more irregular in the middle of the temperature range, whereas Preparation 2 was considerably less robust at high temperatures.

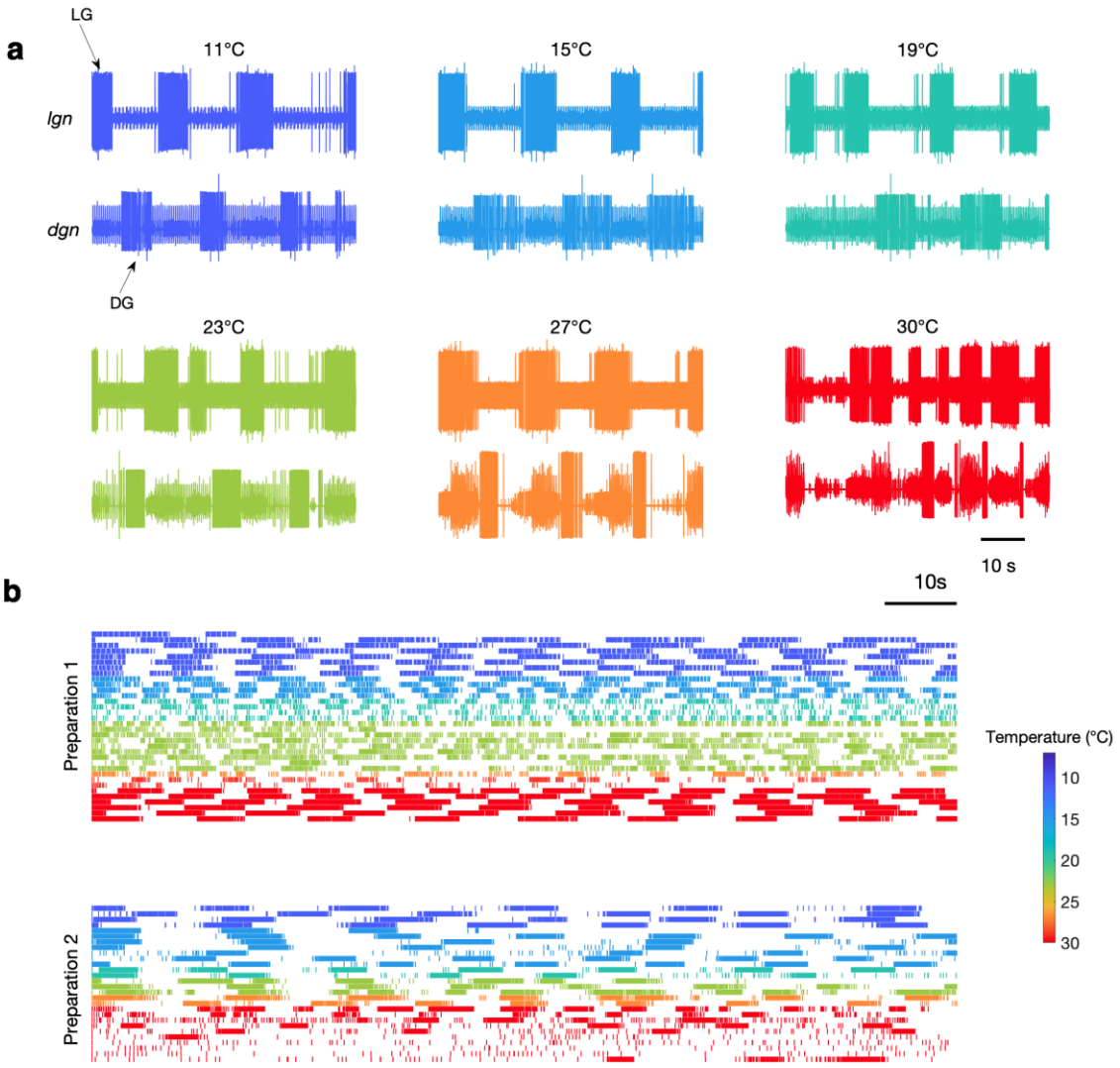

Figure 2. Spontaneous gastric rhythms over physiological temperature range. (**a**) Extracellular recordings from the *lgn* and *dgn* at the temperatures indicated using the color code. (**b**) Spike rasters of LG from two preparations at the indicated colors to show the activity of these preparations over extended periods of time at the indicated temperatures.

Although **Figure 2** only shows two examples of spontaneous gastric mill rhythm, there were a total of ten preparations where spontaneous rhythms were observed at a variety of different temperatures (**Fig. 2–figure supplement 1**). Together, these data

indicate that activating at least some combination of endogenous inputs to the gastric mill circuit can generate rhythmic activity across a wide temperature range. Nonetheless, because the cycle period of the gastric mill was often irregular in these spontaneous rhythms, we were not able to assess whether the pyloric and gastric mill circuits remained coupled. Consequently, we chose to reliably activate gastric rhythms by stimulating a known modulatory pathway (**Methods**), in an attempt to get a more reproducible gastric mill rhythm, of known mechanism, across temperature and across preparations.

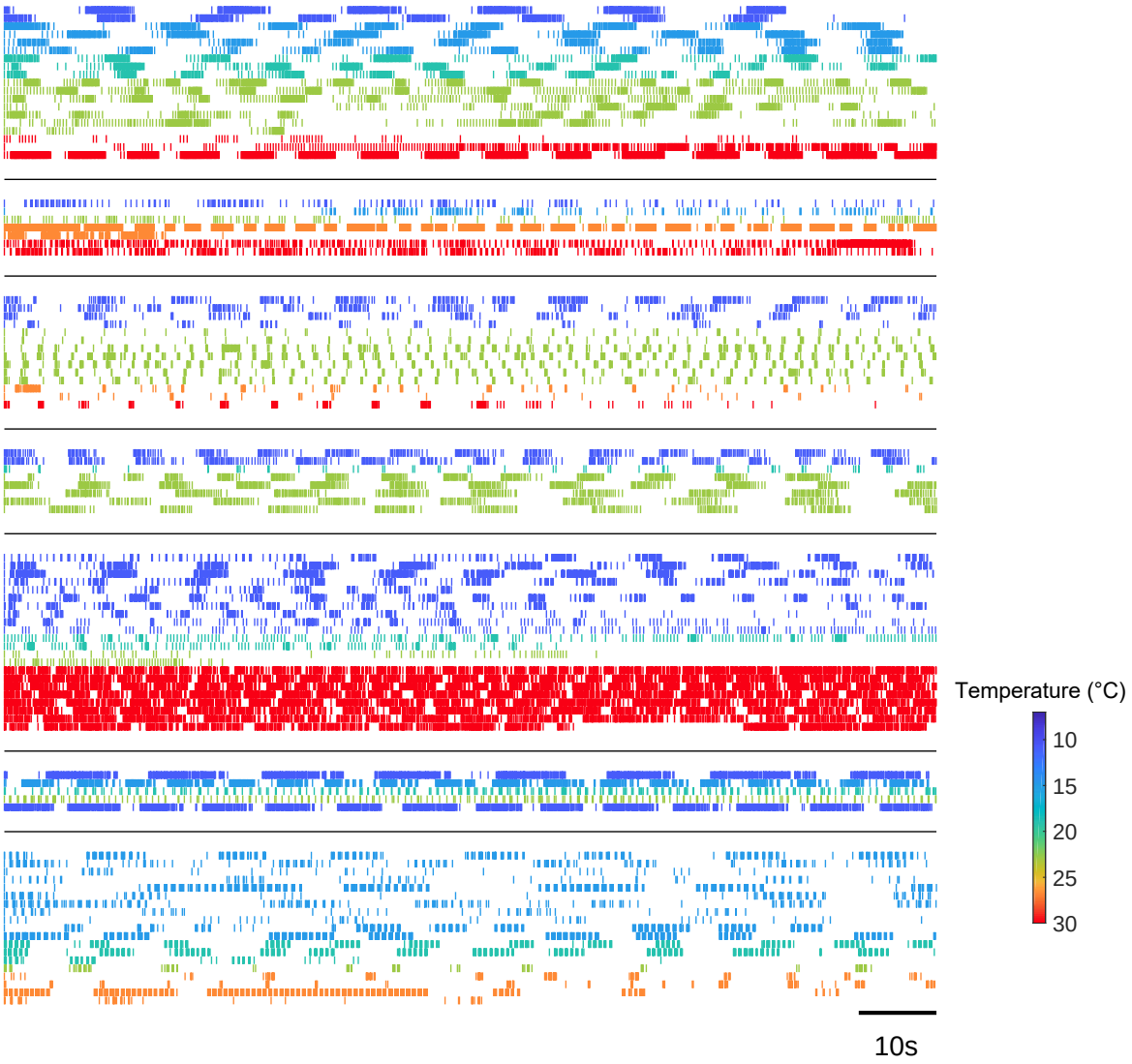

Figure 2–figure supplement 1. Spontaneous gastric activity in seven additional preparations. Each panel shows rasters of LG neurons from a single preparation at temperatures from 11-30°C. LG was spontaneously active at temperatures as high as 30°C. Color of each row of raster indicates temperatures.

Gastric mill rhythm speeds up with increased temperature

We were able to evoke gastric rhythms across the same temperature range at which the pyloric circuit is robust (Tang et al., 2010). **Figure 3** shows example

recordings of evoked gastric rhythms at 7°C (**Fig. 3a**) and 23°C (**Fig. 3b**). Raster plots from this preparation for the extended temperature range are shown in **Figure 3c**. Similar to the pyloric circuit, the gastric mill rhythm cycle period decreased with increased temperature from 7°C to 23°C. Although some of the neuron phase relationships (relative timing of the neurons in each cycle) were altered at 23°C (for example, between DG and LG in **Figure 3b**), at high temperatures, the gastric mill rhythm generator was still producing regular rhythmic activity following stimulation.

We were able to evoke gastric rhythms across a temperature range of 7–21°C in 9/10 preparations.

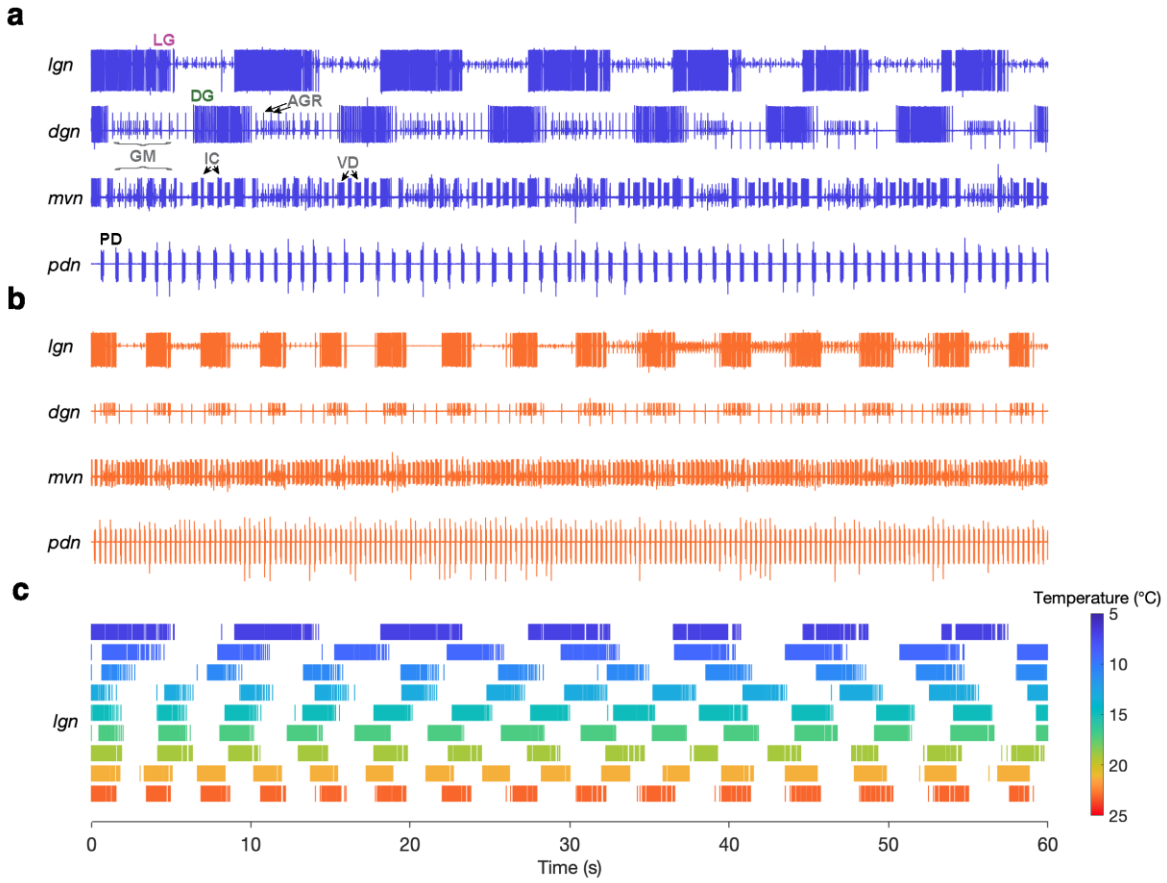

225

226 **Figure 3. Gastric mill rhythms can be evoked by stimulation over**
227 **physiological range.** (**a**) Extracellular recordings from a preparation at 7°C (blue)
228 and (**b**) 23°C (orange). Neuron action potentials described by their relative amplitudes
229 on each nerve: *lgn*: LG (large bursting unit); *dgn*: DG (large, bursting unit; out of phase
230 with LG: only on 7°C trace, has ceased bursting at 23°C), AGR (tonic), GM (small,
231 bursting; in-phase with LG); *mvn*: IC (large), VD (medium, antiphase with LG,
232 alternates with IC), GM (small, bursting; in-phase with LG); *pdn*: PD. (**c**) Spike rasters
233 showing the activity of the LG neuron over the entire temperature range.

234

235 In some preparations (4/10), spontaneous gastric mill rhythms were observed
236 prior to evoking a rhythm. **Figure 3–figure supplement 1a** shows example
237 recordings of both a spontaneous (black) and evoked (blue) gastric mill rhythm from the
238 same preparation (11°C). Three of these four preparations had spontaneous and evoked

239 rhythms shared similarities in LG spike and burst timing (**Fig. 3–figure supplement**
240 **1b**) and rhythm cycle period (mean ± SD) (**Fig. 3–figure supplement 1c**). Because all
241 but two versions of gastric mill rhythms are distinct from one another (Heinzel et al.,
242 1993; Coleman and Nusbaum, 1994; Norris et al., 1996; Weimann et al., 1997; Blitz et
243 al., 1999; Christie et al., 2004; Saideman et al., 2007a; Saideman et al., 2007b; White
244 and Nusbaum, 2011; Dickinson et al., 2015; Blitz et al., 2019), similarities between
245 spontaneous and evoked gastric mill rhythms within a preparation suggested that these
246 rhythms are driven by similar processes.

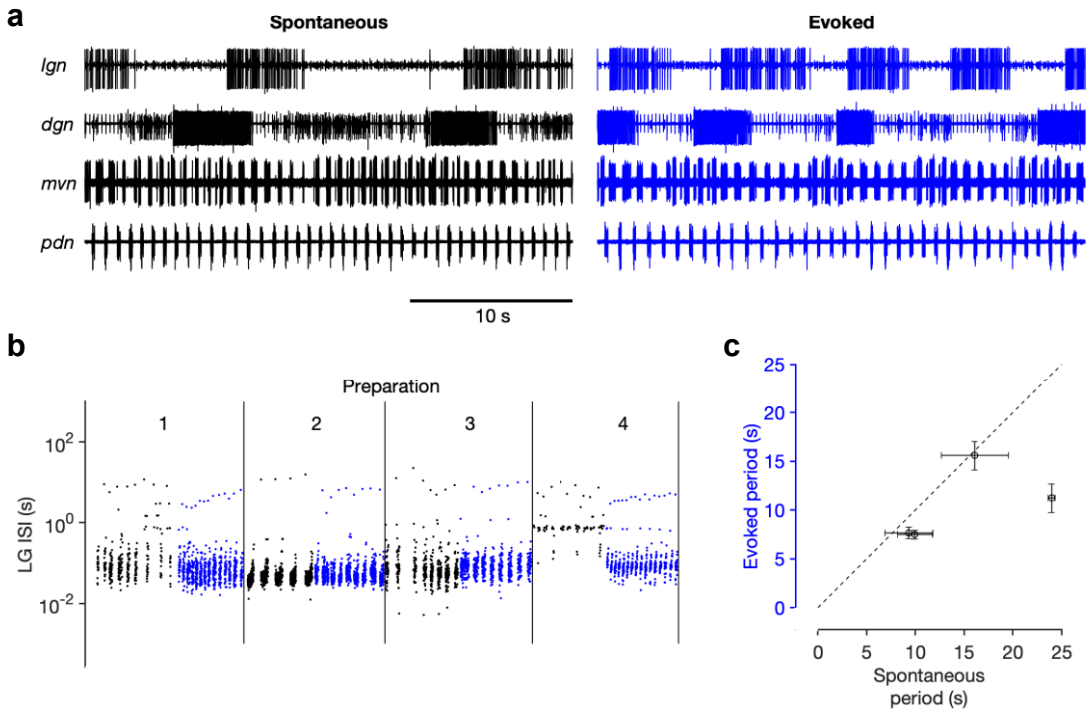

247

248 **Figure 3–figure supplement 1. Comparison of spontaneous and elicited**
249 **gastric activity within the same preparation.** In 4/10 preparations, spontaneous
250 gastric activity was observed at 11°C. (a) Extracellular traces showing activity on lgn,
251 dgn, mvn and pdn nerves during spontaneous gastric activity (black) and after
252 stimulation (blue). (b) Inter-spike intervals (ISIs) of LG neuron in the four preparations
253 that showed spontaneous gastric activity. Black dots indicate ISIs from spontaneous
254 activity and blue dots from evoked activity. (c) Comparison of burst period of LG during
255 spontaneous and evoked bursting.

256 **Gastric mill and pyloric cycle periods are similarly temperature sensitive**

257 The pyloric cycle period decreases ~ 2-fold with a 10°C increase in temperature
258 (Tang et al., 2010). If the pyloric and gastric mill circuits are to be coordinated across
259 temperature perturbations, we hypothesized that the gastric mill period might also show
260 a similar temperature dependence. We measured the burst periods of PD neurons (**Fig**
261 **4, black**) and LG neurons (**Fig 4, magenta**) in all 10 preparations in which the gastric
262 mill rhythm was evoked by stimulation over a temperature range from 7–21°C. **Fig 4a**
263 shows that, in a single preparation, both LG and PD burst periods decrease with
264 increasing temperature, despite significant variability in the LG burst period, due to a
265 slowing down of the gastric mill rhythm with time since stimulation (Beenhakker et al.,
266 2004; Stein et al., 2007).

267 A coordinated decrease in both gastric mill and pyloric cycle periods was
268 observed in all ten preparations (**Fig. 4b**). We quantified the extent to which the cycle
269 period increased with temperature using the Q_{10} (**Methods**). **Figure 4c** shows that
270 most preparations (8 of 10) exhibited a cycle period Q_{10} of ~2 for both pyloric and
271 gastric mill rhythms (paired t-test, $p = 0.136, N = 10$). These data suggest that the
272 periods of both circuits were similarly influenced by increased temperature.

273

274

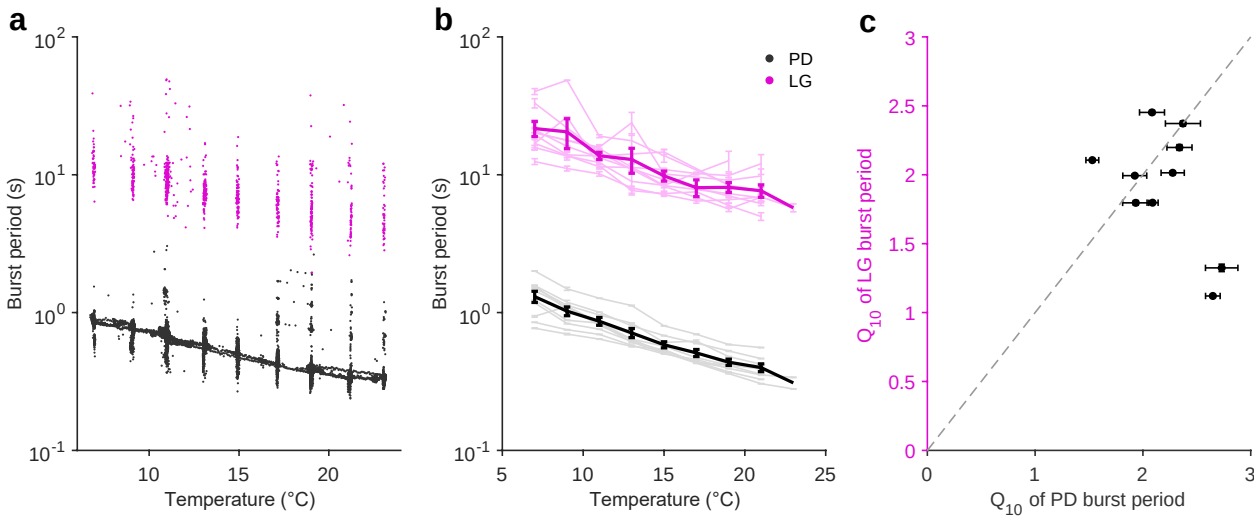

Figure 4. Pyloric and Gastric mill periods are similarly temperature sensitive. (**a**) Burst period of PD (black) and LG (magenta) in a single preparation as a function of temperature. Each dot corresponds to a single burst. (**b**) Burst period of PD and LG for ten preparations. Each line is a single preparation. Mean over all preparations shown in thick lines. (**c**) The apparent Q_{10} of the burst frequency of each preparation for the PD and LG neurons, representing the pyloric and gastric rhythms. The apparent Q_{10}s of the two rhythms are similar (paired *t*-test, $p = 0.136, N = 10$)

Integer coupling is maintained across a physiological temperature range

Integer coupling between two interacting oscillators with different periods refers to the phenomenon that the rhythm with a longer cycle period (gastric mill) tends to be an integer multiple of the shorter cycle period (pyloric) (Nadim et al., 1998). Integer coupling exists between the pyloric and gastric mill oscillators at 11°C (Bartos et al., 1999; Hamood and Marder, 2015). It remains an open question if this form of precise coordination is preserved across temperature, since both oscillators change their cycle periods with temperature.

Raw extracellular recordings of *lgn* and *pdn* at 7°C and 23°C from the same preparation are shown in **Fig. 5a**. PD bursts tended to terminate shortly before the

initiation of LG bursting at both temperatures (**Fig. 5a**, dotted vertical lines indicate start of LG bursting). The ratio of LG to PD periods was close to an integer at both temperatures (~10 at 7°C and ~11 at 23°C).

To visualize integer coupling between the PD and LG across the entire dataset, we plotted the LG burst period as a function of the mean PD burst period during that LG burst (**Fig. 5b**). Data tended to lie along lines with integer slope (gray lines), suggesting integer coupling between LG and PD across temperature. DG burst periods, which were similar to LG burst periods, did not tend to be integer multiples of PD burst periods (**Fig. 5c**). To quantify the degree of integer coupling, we computed the cumulative distribution of significands (value after the decimal point) of the ratios of gastric mill to pyloric periods (**Fig. 5d**, **Methods**). Perfect integer coupling would lead to a cumulative distribution indicated by the dotted line, while randomly chosen significands would lie along the diagonal. Cumulative distributions for LG were skewed towards perfect integer coupling, while distributions for DG were closer to the randomly distributed significands, suggesting that integer coupling was observed in LG, but not DG.

To quantify how the degree of integer coupling varies across temperature, we measured the area between the cumulative distributions and the diagonal in **Fig. 5d**. Perfect integer coupling would yield an area of 0.25. LG and PD were significantly integer coupled at temperatures from 7°C–21°C ($p < 10^{-6}$ paired Kolmogorov-Smirnoff test), while DG and PD were not significantly coupled at any temperature (**Fig. 5e**, **Methods**, paired Kolmogorov-Smirnoff test, corrected for multiple comparisons). Strong integer coupling could arise by regulating the number of PD cycles per LG

period, however previous work shows that the number of pyloric cycles is not a good predictor of gastric mill cycle period (Nadim et al., 1998; Bartos et al., 1999). Instead, AB dictates the phase at which LG turns on because LG onset is timed with the peak of Int1 inhibition (Nadim et al., 1998). Because all previous studies of integer coupling were at ~11°C, it is not known if the process underlying integer coupling would shift with temperature increase. To visualize the effect of temperature on the ratio of PD to LG cycle period, we plotted the ratio of LG cycle period and PD cycle period as a function of temperature (**Fig. 5f**). At low temperatures, when integer coupling was particularly strong (as seen from the vertical banding), these ratios were distributed over a wide range from 5-25. Ratios of LG to PD cycle period were spread across a similar range across temperature, even at higher temperatures when integer coupling degraded ($p = 0.88$, Spearman test), suggesting that the mechanism of integer coupling was independent of the control of the number of PD cycles to LG cycle period.

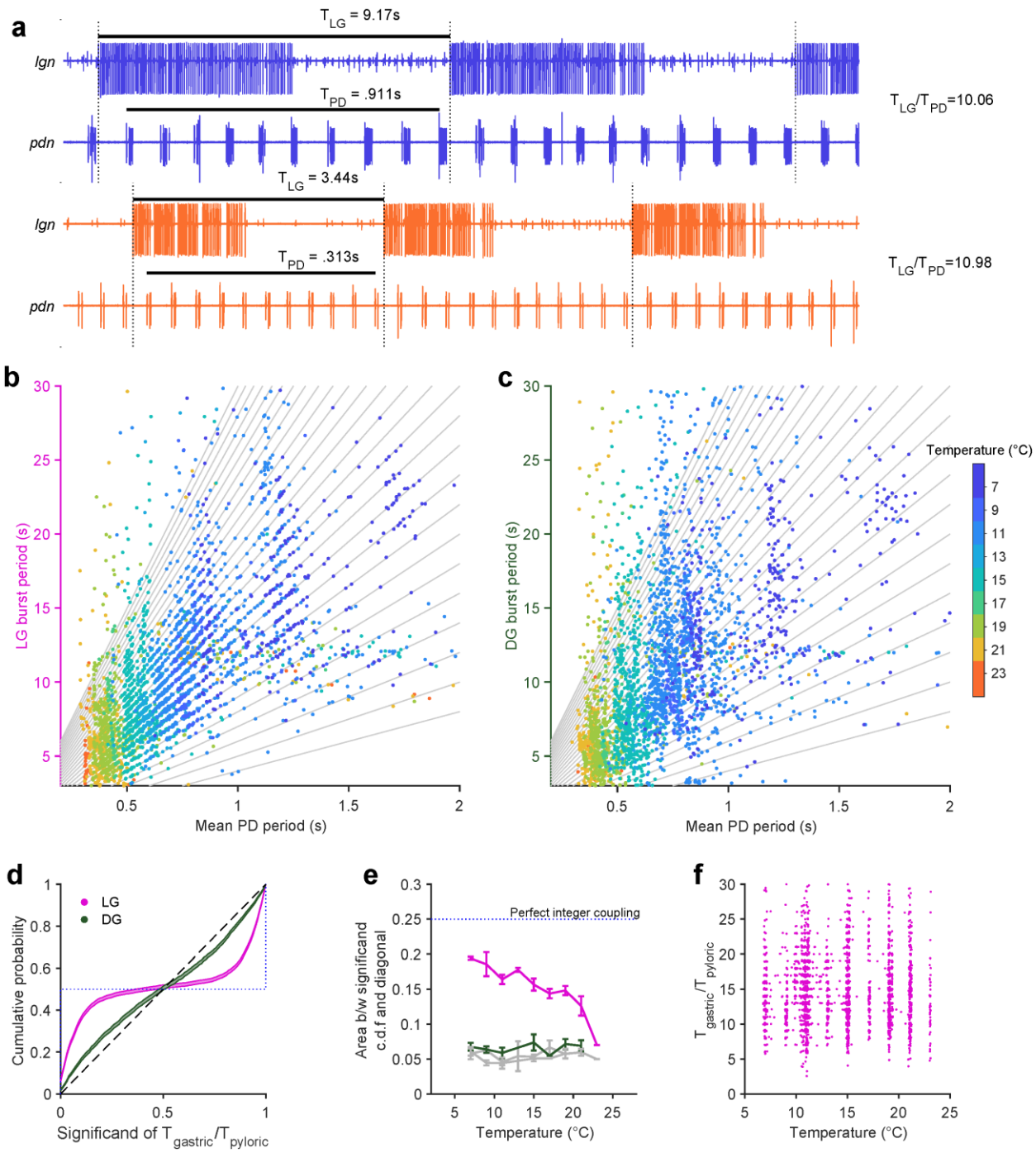

Figure 5. Integer coupling is maintained over physiological range. (**a**) Extracellular recordings of *pdn* show bursting of LG and PD at 7°C (blue) and 23°C (orange). The mean burst period of LG and PD at times indicated by black bars. LG (**b**) and DG (**c**) burst period as a function of mean PD period. In (**b-c**), gray lines have integer slopes, and are not fits. (**d**) Cumulative probability distributions (cdfs) of significand of ratio of gastric to pyloric period for LG (magenta) and DG (green). Dashed diagonal line indicates a uniform distribution, and the dotted line indicates perfect

integer coupling. (**e**) Area between significand cdfs and diagonal (a measure of how integer coupled the circuits are) as a function of temperature for all preparations. Gray lines are data with randomized significands. LG and PD were significantly integer coupled between 7°C–21°C ($p < 10^{-6}$ paired Kolmogorov-Smirnoff test), while DG and PD did not exhibit integer coupling (**f**) Ratio of gastric to pyloric periods as a function of temperature. Apparent banding along the temperature axis is a consequence of the experimental protocol, where discrete temperature steps were used (Methods). Ratios of LG to PD cycle period were similar across temperature ($p = 0.88$, Spearman test).

LG preserves phase locking to PD across physiological temperatures

How do LG and PD maintain integer coupling in their burst periods across this temperature range? One possibility is via temperature-invariant phase locking between LG and PD. If LG bursts start at a particular phase in the PD cycle, then the burst periods of LG and PD must be integer coupled (Nadim et al., 1998). We therefore set out to study the fine structure of the phase coupling between LG and PD across temperature.

To visualize the phase coupling between LG and PD, we plotted PD spikes aligned to LG burst starts (**Fig. 6a**) in a single preparation, normalizing time by the mean PD burst period in each row. Doing so aligned all the PD spikes, suggesting that LG burst starts were an excellent predictor of PD phase. To quantify this effect across all preparations, we computed probabilities of LG bursts starts across the temperature range tested. LG burst start probabilities were sharply peaked (**Fig. 6b**), and were significantly different from a uniform distribution (**Fig. 6b**, dashed line, $p < 10^{-8}$, Kolmogorov-Smirnoff test). Across all temperatures tested, LG started to burst at a phase of ~0.5 in the PD cycle (**Fig. 6b, inset**), and this phase offset was maintained at all temperatures tested ($p = 0.08$, Spearman test).

LG burst initiation being phase locked to PD suggests that faster dynamics in LG such as spiking could also be affected by PD. Modulation of LG spiking by AB/PD has been reported via feedback from AB to MCN1 and CPN2 (Blitz and Nusbaum, 2008) and possibly Int1 feedback to CPN2 (Blitz, 2017). We measured the spike probability of LG conditional on PD phase across this temperature range, and found a pronounced decrease in the probability of spiking in LG at higher temperatures (**Fig. 6c**). This decrease in LG spike probability occurred close to PD burst termination (**Fig. 6c**, horizontal bars). DG, which is not directly coupled to the pyloric oscillator (**Fig. 1**), yet which bursts on the same timescale as LG, shows none of the signatures of phase coupling with PD. DG bursts starts do not align with PD spikes (**Fig. 6d**), and DG burst starts are not sharply peaked in PD phase (**Fig. 6e**). DG spike probability also does not show a noticeable decrease close to the end of PD bursting (**Fig. 6f**).

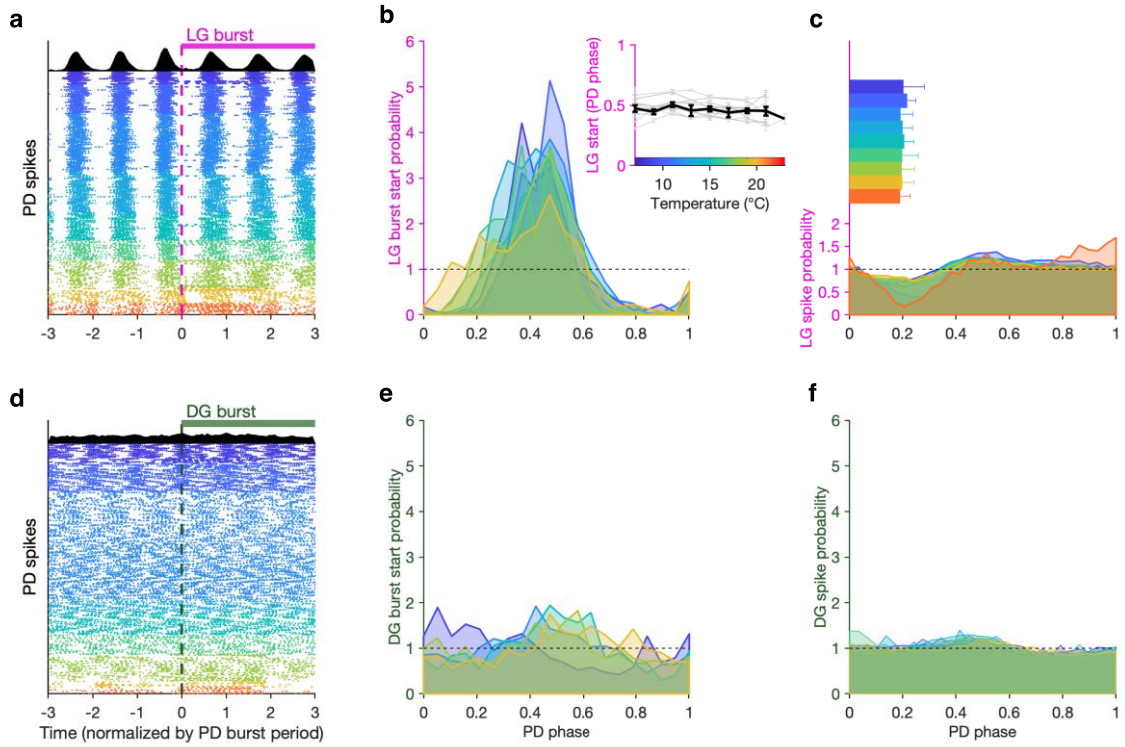

Figure 6. LG, but not DG, bursts and spikes are phase locked to PD across temperature. (**a**) PD spike rasters aligned to LG burst starts (dashed line at 0) in a single preparation. Each row corresponds to a LG burst start, and time is normalized by PD burst period. Histogram shows spike probability over all rasters. (**b**) LG burst start probability as a function of PD phase. Inset shows mean LG burst start phase a function of temperature (gray lines: individual preparations, black line: mean across all preparations). LG burst start probabilities were significantly different from a uniform distribution ($p < 10^{-8}$, Kolmogorov-Smirnoff test). Phase offset between LG and PD was similar at all temperatures tested (inset, $p = 0.08$, Spearman test) (**c**) LG spike probability as a function of PD phase at various temperatures. Bars indicate PD spiking. (**d-f**) Similar to (**a-c**), but for DG.

Discussion

Temperature sensitive circuits maintain coordinated activity

Coupling between rhythmic circuits is common in nervous systems and is often functionally important, although the strength and the extent of inter-circuit coupling is varied (Nadim et al., 1998; Bartos et al., 1999; Colgin, 2011; Gordon, 2011; Jacobson et al., 2013; Rojas-Líbano et al., 2014; Harris and Gordon, 2015; Karalis et al., 2016; Tamura et al., 2017). Temperature is a global perturbation that influences the properties of all ion channels and synapses in neuronal circuits (Zečević et al., 1985; Janssen, 1992; Xu and Meldrum Robertson, 1996; Garrity et al., 2010; Tang et al., 2010; Kang et al., 2012; Robertson and Money, 2012; Marder et al., 2015). Because each cellular and molecular process is likely to have a different temperature dependence, or Q_{10}, maintaining the function of complex physiological processes as temperature is changed is non-trivial (Du et al., 2010; Caplan et al., 2014; Roemschied et al., 2014; O'Leary and Marder, 2016; Schleimer and Schreiber, 2016). Most often, changes in temperature affect neuronal and circuit behavior (Zečević and Levitan, 1980; Prosser and Nelson, 1981; Ramot et al., 2008; Garrity et al., 2010; Robertson and Money, 2012). It then becomes critical to know whether the coupling between circuits is also altered (Stiebler and Narins, 1990), or whether the relative coordination between rhythmic behaviors can be maintained as temperature changes.

Here we show that two oscillator circuits can maintain coordinated output across a range of physiologically relevant temperatures. The cardiac ganglion, another circuit in the crab which governs heartbeat, is also temperature sensitive across a range of physiological temperature, again with a Q_{10} of ~2 (Kushinsky et al., 2019). In the pyloric,

gastric mill, and cardiac circuits, rhythmicity is maintained up to a critical temperature, and this critical temperature approximates the upper range of native ambient temperatures (Tang et al., 2010; Stadele et al., 2015; Kushinsky et al., 2019).

Oscillator circuits with different periods are similarly temperature robust

Although the gastric mill and pyloric rhythms are similarly temperature sensitive, they have an approximately 10-fold difference in cycle period. The pyloric rhythm is temperature robust because the AB neuron maintains a relatively constant duty cycle across this range (Tang et al., 2010; Rinberg et al., 2013). Nonetheless, temperature robustness in the gastric mill rhythm arises from a different set of interdependent processes including projection neuron input, coordination of the half-center oscillator neurons LG and Int1, and feedback from LG to MCN1. The similarity between the apparent cycle period Q_{10}s of the pyloric and gastric mill rhythms is striking as there are so many different physiological processes generating the two rhythms. Moreover, a lock step variance in cycle period is not necessary in order to maintain coupling as the relative number of cycles between each circuits can vary widely while circuits remain coupled (Nadim et al., 1998; Bartos et al., 1999). Because the salient drivers of LG firing are sufficient excitatory drive and inhibition of Int1 (Bartos et al., 1999; DeLong et al., 2009), the total number of pyloric cycles per gastric mill cycle could vary greatly.

Circuits remain coupled across temperature

At temperatures below 20°C, the circuits remain integer coupled. Although integer coupling is lost at higher temperatures, this is not tantamount to a loss of coupling between the two circuits. We know from previous work that when the pyloric rhythm is inhibited, the cycle period of the gastric mill rhythm nearly triples (Bartos et al., 1999). We do not observe an increase in LG cycle period at temperatures where integer coupling is lost. Instead, integer coupling is lost due to a temperature dependent advance of LG burst onset in PD phase, where the LG neuron begins bursting during a PD burst. Therefore, even though integer coupling is lost, AB is still responsible for LG firing across this temperature range.

Coupling between pyloric and gastric mill rhythms was less clear during spontaneous gastric mill rhythms

As spontaneous gastric mill activity was often irregular, it was difficult to examine coupling between the two rhythm generating circuits. Furthermore, the etiology of the spontaneous rhythms was unclear, both within preparations across temperature and across preparations. There are many different processes that drive gastric mill rhythms including release of hormonal peptides: crustacean cardioactive peptide (CCAP) (Weimann et al., 1997), FLRFamides (Heinzel et al., 1993; Weimann et al., 1993; Christie et al., 2004), pyrokinins (Saideman et al., 2007b; Dickinson et al., 2015), and Gly^{1}-SIFamide (Blitz et al., 2019). Synaptically released peptides *C. borealis* tachykinin related peptide (CabTRP Ia) (Blitz et al., 1999; Wood et al., 2000), and *C. borealis* pyrokinin peptide I & II (CabPK) (Saideman et al., 2007a; Saideman et al.,

458 2007b) generate similar gastric mill rhythms, and proctolin (Blitz et al., 1999; Stein et
459 al., 2007) excites all gastric mill motor neurons.

460 Stimulation of certain projection neuron such as MCN1 (contains CabTRP,
461 proctolin, and GABA) (Coleman and Nusbaum, 1994; Coleman et al., 1995; Bartos and
462 Nusbaum, 1997), MCN5 (contains Gly^{1}-SIFamide) (Norris et al., 1996; Blitz et al., 2019),
463 MCN7 (contains proctolin) (Blitz et al., 1999), CPN2 (Norris et al., 1994), and IVN (the
464 inferior ventricular neurons) (contain FLRFamide and histamine) (Christie et al., 2004),
465 or stimulation of sensory pathways that activate groups of projection neurons (Katz and
466 Harris-Warrick, 1991; Beenhakker et al., 2004; Beenhakker and Nusbaum, 2004; Blitz
467 et al., 2004; Beenhakker et al., 2007; White and Nusbaum, 2011) generate gastric mill
468 rhythms. Because there are so many ways gastric mill rhythms can be generated, and
469 because each method of gastric mill rhythm generation could result in a gastric mill
470 rhythm operating using a different set of mechanisms, they could have different
471 temperature dependencies. Consequently, we chose to elicit gastric mill rhythms using
472 a single, known mechanism, and we used exogenous stimulation that would reliably
473 produce gastric mill rhythms, that were qualitatively similar to the spontaneous gastric
474 mill rhythms we had previously observed.

475 A previous study showed that one gastric mill rhythm variant is easily disrupted
476 by small temperature changes (Stadele et al., 2015), while the one studied here
477 maintains rhythmicity following a large increase in temperature. Although the
478 functional significance of the diversity among gastric mill rhythms is unclear, the
479 possibility remains that the assortment of gastric mill rhythm generator mechanisms
480 bequeaths a robustness against environmental perturbation. Because there are other

versions of the gastric mill not considered here, it will be interesting in the future to determine the extent to which they are temperature robust and whether, in turn, they are coupled to the pyloric rhythm across temperature.

Temperature compensation is driven by multiple mechanisms

Previous work has shown that neuromodulatory substances can extend the temperature range over which the gastric and pyloric rhythms maintain function (Stadele et al., 2015; Haddad and Marder, 2018). In *C. elegans* neuromodulation enhances the robustness of thermosensory neurons by increasing the coherence of the temperature range in which they operate (Beverly et al., 2011). Therefore, it is possible that some modulators that act on the STG, not studied here, may further stabilize these rhythms, and one possibility is that some of the modulatory inputs to the STG preferentially release transmitter in response to temperature stress for precisely this reason.

The gastric mill oscillator is activated by both chemical and electrical synapses. In crayfish, the rectifying electrical junction from the lateral giant fiber to the motor giant fiber has reliable synaptic propagation between 20°C and 30°C (Heitler and Edwards, 1998). In a model of this crayfish circuit, Heitler and Edwards (1998) found that if the electrical synapse had a Q_{10} of 11, when most other measured properties of the circuit had Q_{10}s between 2 and 5, the model reliably reproduced physiological responses to temperature increase. At high temperatures, this increased drive from the electrical synapse offsets the decrease in input resistance of the postsynaptic neuron. In the evoked gastric mill rhythms, CPN2 drives LG and GM via electrical synapses (**Figure**

1c), and our spontaneous rhythms, indicative of CPN2 activation, were observed up to 30°C. While we do not know the Q_{10} of electrical synapses in the STG, several measured chemical synapses in the pyloric circuit have a Q_{10} of ~2.5 (Tang et al., 2010).

Previous work shows that input resistance modestly decreases in both the Lateral Pyloric (LP) and LG neurons with increased temperature (Tang et al., 2010; Stadele et al., 2015). The MCN1–LG electrical synapse may help offset the change in input resistance in the gastric circuit. In the pyloric circuit, the IPSP amplitude in the LP neuron is temperature invariant (Q_{10} ~1), but the IPSC amplitude increased (Q_{10} ~2.5) across the same range of temperatures as those studied here (Tang et al., 2010). The increase in synaptic current may partially compensate for the increase in leak as temperature increases. This could aid circuits in maintaining rhythmicity across temperature. Furthermore, many STG neurons, including both LP and LG, exhibit post-inhibitory rebound (PIR). Both I_A and I_h (currents the promote bursting and PIR) exhibit temperature dependent increases in activation rate and peak current (Q_{10}s ~2 – 4) (Tang et al., 2010).

Circuits are robust to global perturbation

Although it may not be uniformly true that all neuronal circuits maintain coordinated function across a wide range of temperatures in cold blooded animals, here we demonstrate that for two coupled circuits where coupling is necessary for proper function, coordination is maintained despite a global perturbation. Because each circuit's oscillations arises from a different set of circuit and cellular mechanisms, it is unlikely that the underlying processes endowing temperature compensation are the

same, and therefore not guaranteed that similar compensation of circuit output for both circuits was to be expected.

The nervous systems of small homeotherms such as birds, rodents (Chaffee and Roberts, 1971; Janssen, 1992), and even human infants (Mank et al., 2016; Barbi et al., 2017) likely face similar challenges as a result of fluctuations in ambient temperature or in fever response to illness. Although they have homeostatic processes that regulate internal temperature shifts, these regulatory responses can be slow compared to temperature change (Cheshire, 2016). Therefore, it is likely that their nervous systems must be robust to some degree of temperature fluctuation in order to maintain function until a homeostatic process can intervene to restore internal temperature.

In this study, we use temperature as a global perturbation. It is possible that coupled neural circuits are similarly robust to other global perturbations so that coupling is maintained despite transient or chronic changes in ambient conditions. For example, the pyloric oscillator is known to be robust to large changes in pH (Haley et al., 2018) and to fluctuations in extracellular potassium (He et al., 2020). Collectively, these data indicate that the crustacean STG (and likely many other neural circuits) are capable of sustaining normal output when challenged with global perturbations. While the processes that confer robustness are probably different for different circuits and perturbations, nervous systems have likely evolved to cope with a variety of environmental changes.

548 **Methods**

549 **Animals and dissection**

550 Adult male Jonah crabs (*C. borealis*; *N* = 20 were obtained from Commercial Lobster
551 (Boston, MA) and kept in tanks with circulating artificial sea water at 11°C for
552 approximately one week prior to use. Preparations with spontaneous rhythms (*N* = 10),
553 crabs were caught in July of 2013 and studied soon thereafter. Preparations in which
554 rhythms were evoked (*N* = 10) were from crabs caught July, Sept., and Dec. of 2017).
555 Thirty minutes prior to dissection, animals were chilled on ice. Dissections were carried
556 out as previously described (Gutierrez and Grashow, 2009) and the dissected nervous
557 systems were kept in chilled saline solution (440 mM NaCl, 11 mM KCl, 26 mM $MgCl_2$,
558 13 mM $CaCl_2$, 11 mM Trizma base, 5 mM maleic acid, pH 7.45 at 23°C) throughout the
559 dissection. Each dissected stomatogastric nervous system was pinned out in a petri dish
560 with a Sylgard-lined bottom and fresh saline was continuously superfused across the
561 nervous system for the duration of the experiment (**Fig. 1a**).

562 ***Nerve Recordings***

563 Motor neuron action potentials originating in the STG (**Fig. 1a**) were recorded
564 extracellularly (**Fig. 1b**) from the nerves via stainless steel pin electrodes. Stretches of
565 the *lgn*, *dgn*, *mvn*, *lvn*, and *pdn* were electrically isolated from the bath with Vaseline
566 wells. Voltage signals were amplified using model 3500 amplifiers (A-M Systems) and
567 digitized at 10 kHz using a Digidata 1440 A-D converter (Axon Instruments/ Molecular
568 Devices). Data were recorded using pClamp data acquisition software (Axon
569 Instruments/Molecular Devices, version 10.5).

Temperature Control

Saline temperature was monitored continuously using a temperature controller (model CL-100, Warner Instruments) and altered during each experiment using an associated Peltier device and thermocouple (SC-20 and TA-29, Warner Instruments). Saline inflow to the nervous system was positioned within 1 cm of the STG so that the measured temperature at the point of inflow was approximately that of the ganglion somata.

Gastric Mill Rhythm Stimulation

We bilaterally stimulated the dorsal posterior esophageal nerves (*dpons*) to elicit a gastric mill rhythm (**Figure 1a & b**). Stainless steel pin electrodes were placed on either side of each *dpon* and were sealed to the nerve using Vaseline. Stimuli were delivered using a model 3800 stimulator (A-M Systems) via model 3820 stimulus isolation units (A-M Systems). Stimuli were delivered in episodic trains (0.6 Hz) and the within train stimulus rate was 15 Hz, as described in Beenhakker and Nusbaum (2004). The *dpons* contain axons of the ventral cardiac neurons (VCNs) that activate the MCN1 and CPN2. MCN1 and CPN2 excite gastric mill and pyloric neurons in the STG. Stimulating the *dpons* for 2 minutes evokes a VCN-gastric mill rhythm that is often active for tens of minutes (Beenhakker et al., 2004; Beenhakker and Nusbaum, 2004; Blitz and Nusbaum, 2008). The duration of each stretch of gastric mill activity is not consistent either within an experiment at different temperatures or across experiments at the same temperature. Thus, the time between each gastric mill rhythm stimulation was different both between temperatures and across preparations. Generally, the amount of time at each temperature step was far longer (~10-20 minutes) than between steps (~2 minutes).

Defining gastric mill rhythm variants

While evoked gastric mill rhythms are distinguished by the method used to drive them, in the case of spontaneous gastric mill rhythms, the phase relationships and timing of the gastric mill neurons are used to classify them (White and Nusbaum, 2011).

Recordings from the *mvn* show the Inferior Cardiac (IC) neuron and ventricular dilator (VD) neuron (**Fig. 1b**). Although in the absence of a gastric mill rhythm, the IC and VD neurons are typically active in time with the LP neuron and the Pyloric neurons (PY_5; there are approximately five PY neurons in each preparation) respectively, the initiation of a gastric mill rhythm will often shift the IC and VD neurons into gastric mill timing as shown in **Figure 1b**. Because the timing of the IC and VD neurons are state-dependent, they can aid in classifying spontaneous gastric mill rhythms.

In this study, spontaneous gastric mill rhythms resemble VCN-rhythms as IC and VD activity is restricted to the LG interburst interval, which is known to occur because of CPN2 and LG inhibition of the IC and VD neurons respectively. Additionally, the LG bursts in these spontaneous rhythms did not exhibit any obvious interruptions, as is the case in another gastric mill rhythm that is similar to a VCN-rhythm, save for this difference (White and Nusbaum, 2011).

Spontaneous and evoked gastric mill rhythm temperature ranges

In one set of experiments ($N = 10$), spontaneous gastric mill rhythms were observed. Here temperature was increased from 11°C to 33°C in 2°C increments, and a given temperature step was held for at least 2 minutes. Time between steps was ~ 2 minutes.

For experiments in which gastric mill rhythms were evoked ($N = 10$), the temperature was increased in either 2°C or 4°C steps starting at 7°C until a gastric mill rhythm could no longer be evoked (typically 21°C or 23°C). Each temperature step was held for the duration of evoked gastric mill activity, and only after the epoch of the gastric mill rhythm terminated was the temperature advanced to the next step. The time between temperature steps was ~ 2 minutes. Data collected during the periods when the temperature was rapidly changed were excluded from the analysis.

The VCN-gastric mill rhythms were difficult to generate consistently above 23°C, and in some cases only persisted for several cycles. In some preparations, 19°C was the warmest temperature that a gastric mill rhythm could be evoked. Because the stimulation paradigm only activates a subset of projection neurons in the CoGs, these manipulations may fail to characterize the full extent to which the gastric mill circuit can maintain rhythmicity across temperature. Within the temperature range in which they were readily evoked, gastric mill rhythms lasted for tens of minutes.

Data analysis

Spike identification and sorting

To reliably identify spikes from extracellular traces, we wrote spike sorting software that uses supervised machine learning to learn the shape of spikes from a small manually labelled dataset. This software is freely available at https://github.com/sg-s/crabsort. PD, LG and DG neuron spikes were identified on the *pdn*, *lgn* and *dgn* nerves recorded extracellularly. In a small subset of the full data, spikes from these neurons were

identified using thresholding, dimensionality reduction of the full spike shape, and manual labelling. Using this subset, we trained a fully connected neural network to classify putative identified spikes in new data. The accuracy of the classification was constantly monitored during sorting, and new annotations were used to continuously re-train the network using an active learning framework. Classification accuracy always exceeded 98%.

After the neural network classified putative spikes in a new dataset, to ensure high-quality spike annotation: 1) we manually inspected the data in two-minute chunks to ensure that no artifacts were accidentally labelled as spikes; 2) we used tools built-in to the spike sorting software to visually inspect, at high-temporal resolution, spikes that the neural network reported low confidence in; and 3) we used other built-in tools to inspect spikes that differed statistically from other spikes in its class. These steps let us generate high-quality spike annotations for PD, LG, and DG, even when these neurons were partially obscured by other units or noise.

Detection of bursts and measurement of burst metrics

Bursts in PD, LG or DG were defined using inter-spike intervals (ISIs). ISIs longer than 1 second on LG or DG were defined to be an inter-burst interval and were used to annotate the start of a burst. Spikes were considered to be part of a burst only if there were at least n spikes per burst, with $n = 5$ for LG and DG and $n = 2$ for PD.

This method allowed us to identify all burst starts, burst stops, and therefore burst durations and burst periods for every burst. We computed the duty cycle on a cycle-by-cycle basis by dividing the burst duration by the burst period.

Estimation of Q_{10}s

The Q_{10} of a process is defined as the factor by which it changes over a ten degree increment in temperature. We computed the Q_{10} of PD and LG burst periods at every temperature (**Fig. 4**) using

$$Q_{10} = \langle \left(\frac{f_T}{f_{11}}\right)^{\frac{10}{T-11}} \rangle$$

where f_T is the mean burst frequency at temperature T and f_{11} is the mean burst frequency at 11°C (the reference temperature).

Generation of burst-aligned rasters of PD

To visualize the interaction between pyloric and gastric mill rhythms, we generated burst-aligned rasters of the PD neuron activity in which we aligned PD rasters to the burst start in a gastric mill-timed neuron (LG or DG). For every burst start in LG/DG, we plotted the raster of PD spikes centered around that burst start, showing spikes two seconds before the burst start in LG/DG and two seconds after.

Integer coupling analysis

To measure the integer coupling between PD burst periods and LG or DG burst periods (**Fig. 5b, c**), we computed the mean burst period of all PD bursts within one LG/DG burst period. Thus, every LG/DG burst period is represented by a dot, with LG/DG burst

period plotted on the vertical axis and the mean PD burst period plotted on the horizontal axis.

To determine if these burst periods are significantly integer coupled (**Fig. 5d**), we computed the significand (defined here as the value after the decimal point) of the ratio of the ordinate to the abscissa for each dot. For example, if an LG burst had a period of 10.1 seconds, and the mean PD period during that LG burst was 1 second, the significand would be 0.1. If the LG burst period was 9.9 seconds, the significant would also be 0.1. We sorted all significands for LG and DG and bootstrapped the data 1000 times to estimate confidence intervals of cumulative density functions of the significands. Curves that deviated substantially from the diagonal (the null distribution) corresponded to significant integer coupling between the gastric mill and pyloric burst periods.

The dotted and dashed lines in **Fig. 5d** indicate two extremes of the significand distribution. If the gastric and pyloric burst periods were perfectly integer coupled, then every significand of every ratio of periods would be 0 (or 1). Thus, the cumulative probability of such an idealized distribution would be a step-like function shown by the dotted line. On the other extreme, if the ratios of gastric to pyloric burst periods was such that the significands were randomly and uniformly distributed across the unit line (suggesting no integer coupling whatsoever), then the cumulative probability of such a distribution would be a diagonal line with unit slope, shown by the dashed line.

These two extremes allow us to define a yardstick to measure the degree of integer coupling for any observed spike train. We observe that all possible cumulative distributions are bounded by the two extremal distributions (dotted line and dashed line). Because the area of the square in **Fig. 5d** is 1, simple geometry tells us that the

area bounded by the maximal distributions is 0.25. We therefore quantified the integer coupling of the two burst periods (**Fig. 5e**) by measuring the area between the null distribution (dashed diagonal line) and the perfectly integer coupled data (dotted line).

Estimation of gastric mill spike and burst start probability in PD phase

To estimate when the LG or DG neurons start bursting in the PD cycle (**Fig. 6**), we first identified the burst start times of LG and DG. At these points, we estimated the PD phase by dividing the time since the start of the previous PD burst by the burst period of that PD cycle. This method of phase estimation assumes that the phase increases uniformly and linearly over a PD cycle, following earlier work (Prinz et al., 2004; Bucher et al., 2005).

References

Bahramisharif A, Mazaheri A, Levar N, Richard Schuurman P, Figee M, Denys D (2016) Deep Brain Stimulation Diminishes Cross-Frequency Coupling in Obsessive-Compulsive Disorder. Biol Psychiatry 80:e57-58.

Barbi E, Marzuillo P, Neri E, Naviglio S, Krauss BS (2017) Fever in Children: Pearls and Pitfalls. Children (Basel) 4:81.

Bartos M, Nusbaum MP (1997) Intercircuit control of motor pattern modulation by presynaptic inhibition. J Neurosci 17:2247-2256.

Bartos M, Manor Y, Nadim F, Marder E, Nusbaum MP (1999) Coordination of fast and slow rhythmic neuronal circuits. J Neurosci 19:6650-6660.

Beenhakker MP, Nusbaum MP (2004) Mechanosensory activation of a motor circuit by coactivation of two projection neurons. J Neurosci 24:6741-6750.

Beenhakker MP, Blitz DM, Nusbaum MP (2004) Long-lasting activation of rhythmic neuronal activity by a novel mechanosensory system in the crustacean stomatogastric nervous system. J Neurophysiol 91:78-91.

Beenhakker MP, Kirby MS, Nusbaum MP (2007) Mechanosensory gating of proprioceptor input to modulatory projection neurons. J Neurosci 27:14308-14316.

Beverly M, Anbil S, Sengupta P (2011) Degeneracy and neuromodulation among thermosensory neurons contribute to robust thermosensory behaviors in Caenorhabditis elegans. J Neurosci 31:11718-11727.

Blitz DM (2017) Circuit feedback increases activity level of a circuit input through interactions with intrinsic properties. J Neurophysiol 118:949-963.

Blitz DM, Nusbaum MP (2008) State-dependent presynaptic inhibition regulates central pattern generator feedback to descending inputs. J Neurosci 28:9564-9574.

Blitz DM, Nusbaum MP (2012) Modulation of circuit feedback specifies motor circuit output. J Neurosci 32:9182-9193.

Blitz DM, Beenhakker MP, Nusbaum MP (2004) Different sensory systems share projection neurons but elicit distinct motor patterns. J Neurosci 24:11381-11390.

Blitz DM, Christie AE, Cook AP, Dickinson PS, Nusbaum MP (2019) Similarities and differences in circuit responses to applied Gly(1)-SIFamide and peptidergic (Gly(1)-SIFamide) neuron stimulation. J Neurophysiol 121:950-972.

Blitz DM, Christie AE, Coleman MJ, Norris BJ, Marder E, Nusbaum MP (1999) Different proctolin neurons elicit distinct motor patterns from a multifunctional neuronal network. J Neurosci 19:5449-5463.

Bucher D, Prinz AA, Marder E (2005) Animal-to-Animal Variability in Motor Pattern Production in Adults and during Growth. The Journal of Neuroscience 25:1611-1619.

Burrows M (1989) Effects of temperature on a central synapse between identified motor neurons in the locust. Journal of Comparative Physiology A 165:687-695.

Cao XJ, Oertel D (2005) Temperature affects voltage-sensitive conductances differentially in octopus cells of the mammalian cochlear nucleus. J Neurophysiol 94:821-832.

Caplan JS, Williams AH, Marder E (2014) Many parameter sets in a multicompartment model oscillator are robust to temperature perturbations. J Neurosci 34:4963-4975.

Chaffee RRJ, Roberts JC (1971) Temperature Acclimation in Birds and Mammals. Annual Review of Physiology 33:155-202.

Cheshire WP (2016) Thermoregulatory disorders and illness related to heat and cold stress. Autonomic Neuroscience 196:91-104.

Christie AE, Stein W, Quinlan JE, Beenhakker MP, Marder E, Nusbaum MP (2004) Actions of a histaminergic/peptidergic projection neuron on rhythmic motor patterns in the stomatogastric nervous system of the crab Cancer borealis. J Comp Neurol 469:153-169.

759 Coleman MJ, Nusbaum MP (1994) Functional consequences of compartmentalization of synaptic input. J
760 Neurosci 14:6544-6552.
761 Coleman MJ, Meyrand P, Nusbaum MP (1995) A switch between two modes of synaptic transmission
762 mediated by presynaptic inhibition. Nature 378:502-505.
763 Colgin LL (2011) Oscillations and hippocampal–prefrontal synchrony. Current Opinion in Neurobiology
764 21:467-474.
765 de Hemptinne C, Ryapolova-Webb ES, Air EL, Garcia PA, Miller KJ, Ojemann JG, Ostrem JL, Galifianakis
766 NB, Starr PA (2013) Exaggerated phase-amplitude coupling in the primary motor cortex in
767 Parkinson disease. Proc Natl Acad Sci U S A 110:4780-4785.
768 DeLong ND, Kirby MS, Blitz DM, Nusbaum MP (2009) Parallel regulation of a modulator-activated
769 current via distinct dynamics underlies comodulation of motor circuit output. J Neurosci
770 29:12355-12367.
771 Dickinson PS, Kurland SC, Qu X, Parker BO, Sreekrishnan A, Kwiatkowski MA, Williams AH, Ysasi AB,
772 Christie AE (2015) Distinct or shared actions of peptide family isoforms: II. Multiple pyrokinins
773 exert similar effects in the lobster stomatogastric nervous system. J Exp Biol 218:2905-2917.
774 Du Y, Lu Q, Wang R (2010) Using interspike intervals to quantify noise effects on spike trains in
775 temperature encoding neurons. Cognitive Neurodynamics 4:199-206.
776 Fohlmeister JF, Cohen ED, Newman EA (2010) Mechanisms and distribution of ion channels in retinal
777 ganglion cells: using temperature as an independent variable. J Neurophysiol 103:1357-1374.
778 Fonseca PJ, Correia T (2007) Effects of temperature on tuning of the auditory pathway in the cicada
779 Tettigetta josei (*Hemiptera, Tibicinidae*). J Exp Biol 210:1834-1845.
780 Foster JA, Robertson RM (1992) Temperature Dependency of Wing-Beat Frequency in Intact and
781 Deafferented Locusts. Journal of Experimental Biology 162:295-312.
782 Franz A, Ronacher B (2002) Temperature dependence of temporal resolution in an insect nervous
783 system. Journal of Comparative Physiology A 188:261-271.
784 Fujisawa S, Buzsaki G (2011) A 4 Hz oscillation adaptively synchronizes prefrontal, VTA, and hippocampal
785 activities. Neuron 72:153-165.
786 Garrity PA, Goodman MB, Samuel AD, Sengupta P (2010) Running hot and cold: behavioral strategies,
787 neural circuits, and the molecular machinery for thermotaxis in *C. elegans* and *Drosophila*.
788 Genes & Development 24:2365-2382.
789 Gordon JA (2011) Oscillations and hippocampal-prefrontal synchrony. Current opinion in neurobiology
790 21:486-491.
791 Gutierrez GJ, Grashow RG (2009) *Cancer borealis* stomatogastric nervous system dissection. J Vis
792 Exp:https://www.ncbi.nlm.nih.gov/pubmed/19308017.
793 Haddad SA, Marder E (2018) Circuit Robustness to Temperature Perturbation Is Altered by
794 Neuromodulators. Neuron 100:609-623 e603.
795 Haley JA, Hampton D, Marder E (2018) Two central pattern generators from the crab, Cancer borealis,
796 respond robustly and differentially to extreme extracellular pH. Elife 7.
797 Hamood AW, Marder E (2015) Consequences of acute and long-term removal of neuromodulatory input
798 on the episodic gastric rhythm of the crab Cancer borealis. J Neurophysiol 114:1677-1692.
799 Harris AZ, Gordon JA (2015) Long-range neural synchrony in behavior. Annu Rev Neurosci 38:171-194.
800 Hazel JR, Prosser CL (1974) Molecular mechanisms of temperature compensation in poikilotherms.
801 Physiol Rev 54:620-677.
802 He LS, Rue MCP, Morozova EO, Powell DJ, James EJ, Kar M, Marder E (2020) Rapid adaptation to
803 elevated extracellular potassium in the pyloric circuit of the crab, *Cancer borealis*. Journal of
804 Neurophysiology 123:2075-2089.

Heinzel HG, Weimann JM, Marder E (1993) The behavioral repertoire of the gastric mill in the crab, Cancer pagurus: an in situ endoscopic and electrophysiological examination. J Neurosci 13:1793-1803.

Heitler WJ, Edwards DH (1998) Effect of temperature on a voltage-sensitive electrical synapse in crayfish. The Journal of Experimental Biology 201:503.

Jacobson TK, Howe MD, Schmidt B, Hinman JR, Escabi MA, Markus EJ (2013) Hippocampal theta, gamma, and theta-gamma coupling: effects of aging, environmental change, and cholinergic activation. J Neurophysiol 109:1852-1865.

Janssen R (1992) Thermal influences on nervous system function. Neuroscience & Biobehavioral Reviews 16:399-413.

Kang K, Panzano VC, Chang EC, Ni L, Dainis AM, Jenkins AM, Regna K, Muskavitch MAT, Garrity PA (2012) Modulation of TRPA1 thermal sensitivity enables sensory discrimination in *Drosophila*. Nature 481:76-80.

Karalis N, Dejean C, Chaudun F, Khoder S, Rozeske RR, Wurtz H, Bagur S, Benchenane K, Sirota A, Courtin J, Herry C (2016) 4-Hz oscillations synchronize prefrontal–amygdala circuits during fear behavior. Nature Neuroscience 19:605-612.

Katz PS, Harris-Warrick RM (1991) Recruitment of crab gastric mill neurons into the pyloric motor pattern by mechanosensory afferent stimulation. J Neurophysiol 65:1442-1451.

Kirihara K, Rissling AJ, Swerdlow NR, Braff DL, Light GA (2012) Hierarchical organization of gamma and theta oscillatory dynamics in schizophrenia. Biol Psychiatry 71:873-880.

Klockner U, Schiefer A, Isenberg G (1990) L-type Ca-channels: similar Q10 of Ca-, Ba- and Na-conductance points to the importance of ion-channel interaction. Pflugers Arch 415:638-641.

Kushinsky D, Morozova EO, Marder E (2019) In vivo effects of temperature on the heart and pyloric rhythms in the crab *Cancer borealis*. J Exp Biol 222.

Lisman J (2005) The theta/gamma discrete phase code occuring during the hippocampal phase precession may be a more general brain coding scheme. Hippocampus 15:913-922.

Lisman J, Buzsáki G (2008) A Neural Coding Scheme Formed by the Combined Function of Gamma and Theta Oscillations. Schizophrenia Bulletin 34:974-980.

Lisman JE, Jensen O (2013) The θ-γ neural code. Neuron 77:1002-1016.

Mank A, van Zanten HA, Meyer MP, Pauws S, Lopriore E, Te Pas AB (2016) Hypothermia in Preterm Infants in the First Hours after Birth: Occurrence, Course and Risk Factors. PLoS One 11:e0164817-e0164817.

Marder E, Bucher D (2007) Understanding circuit dynamics using the stomatogastric nervous system of lobsters and crabs. Annu Rev Physiol 69:291-316.

Marder E, Manor Y, Nadim F, Bartos M, Nusbaum MP (1998) Frequency control of a slow oscillatory network by a fast rhythmic input: pyloric to gastric mill interactions in the crab stomatogastric nervous system. Ann N Y Acad Sci 860:226-238.

Marder E, Haddad SA, Goeritz ML, Rosenbaum P, Kispersky T (2015) How can motor systems retain performance over a wide temperature range? Lessons from the crustacean stomatogastric nervous system. J Comp Physiol A Neuroethol Sens Neural Behav Physiol 201:851-856.

Montgomery SM, Buzsaki G (2007) Gamma oscillations dynamically couple hippocampal CA3 and CA1 regions during memory task performance. Proc Natl Acad Sci U S A 104:14495-14500.

Moran LV, Hong LE (2011) High vs low frequency neural oscillations in schizophrenia. Schizophr Bull 37:659-663.

Moran MM, Xu H, Clapham DE (2004) TRP ion channels in the nervous system. Curr Opin Neurobiol 14:362-369.

Nadim F, Manor Y, Nusbaum MP, Marder E (1998) Frequency regulation of a slow rhythm by a fast periodic input. J Neurosci 18:5053-5067.

Norris BJ, Coleman MJ, Nusbaum MP (1994) Recruitment of a projection neuron determines gastric mill motor pattern selection in the stomatogastric nervous system of the crab, Cancer borealis. J Neurophysiol 72:1451-1463.
Norris BJ, Coleman MJ, Nusbaum MP (1996) Pyloric motor pattern modification by a newly identified projection neuron in the crab stomatogastric nervous system. J Neurophysiol 75:97-108.
O'Leary T, Marder E (2016) Temperature-Robust Neural Function from Activity-Dependent Ion Channel Regulation. Curr Biol 26:2935-2941.
Prinz AA, Bucher D, Marder E (2004) Similar network activity from disparate circuit parameters. Nat Neurosci 7:1345-1352.
Prosser CL, Nelson DO (1981) The Role of Nervous Systems in Temperature Adaptation of Poikilotherms. Annual Review of Physiology 43:281-300.
Ramot D, MacInnis BL, Goodman MB (2008) Bidirectional temperature-sensing by a single thermosensory neuron in *C. elegans*. Nature Neuroscience 11:908-915.
Rinberg A, Taylor AL, Marder E (2013) The effects of temperature on the stability of a neuronal oscillator. PLoS Comput Biol 9:e1002857.
Robertson RM, Money TGA (2012) Temperature and neuronal circuit function: compensation, tuning and tolerance. Current Opinion in Neurobiology 22:724-734.
Roemschied FA, Eberhard MJB, Schleimer J-H, Ronacher B, Schreiber S (2014) Cell-intrinsic mechanisms of temperature compensation in a grasshopper sensory receptor neuron. eLife 3:e02078.
Rojas-Líbano D, Frederick DE, Egaña JI, Kay LM (2014) The olfactory bulb theta rhythm follows all frequencies of diaphragmatic respiration in the freely behaving rat. Front Behav Neurosci 8:214-214.
Saideman SR, Blitz DM, Nusbaum MP (2007a) Convergent motor patterns from divergent circuits. J Neurosci 27:6664-6674.
Saideman SR, Ma M, Kutz-Naber KK, Cook A, Torfs P, Schoofs L, Li L, Nusbaum MP (2007b) Modulation of rhythmic motor activity by pyrokinin peptides. J Neurophysiol 97:579-595.
Salimpour Y, Anderson WS (2019) Cross-Frequency Coupling Based Neuromodulation for Treating Neurological Disorders. Frontiers in Neuroscience 13.
Scheffer-Teixeira R, Tort ABL (2016) On cross-frequency phase-phase coupling between theta and gamma oscillations in the hippocampus. eLife 5:e20515.
Schleimer J-H, Schreiber S (2016) Homeostasis: How Neurons Achieve Temperature Invariance. Current Biology 26:R1141-R1143.
Soofi W, Goeritz ML, Kispersky TJ, Prinz AA, Marder E, Stein W (2014) Phase maintenance in a rhythmic motor pattern during temperature changes in vivo. J Neurophysiol 111:2603-2613.
Stadele C, Heigele S, Stein W (2015) Neuromodulation to the Rescue: Compensation of Temperature-Induced Breakdown of Rhythmic Motor Patterns via Extrinsic Neuromodulatory Input. PLoS Biol 13:e1002265.
Stehlik LL, MacKenzie Jr. CL, Morse WW (1991) Distribution and abundance of four brachyuran crabs on the northwest atlantic shelf. Fishery Bulletin, US:473-492.
Stein W, DeLong ND, Wood DE, Nusbaum MP (2007) Divergent co-transmitter actions underlie motor pattern activation by a modulatory projection neuron. Eur J Neurosci 26:1148-1165.
Stiebler IB, Narins PM (1990) Temperature-dependence of auditory nerve response properties in the frog. Hearing Research 46:63-81.
Tamura M, Spellman TJ, Rosen AM, Gogos JA, Gordon JA (2017) Hippocampal-prefrontal theta-gamma coupling during performance of a spatial working memory task. Nature Communications 8:2182.
Tang LS, Taylor AL, Rinberg A, Marder E (2012) Robustness of a rhythmic circuit to short- and long-term temperature changes. J Neurosci 32:10075-10085.

Tang LS, Goeritz ML, Caplan JS, Taylor AL, Fisek M, Marder E (2010) Precise temperature compensation of phase in a rhythmic motor pattern. PLoS Biol 8.

Tass P, Rosenblum MG, Weule J, Kurths J, Pikovsky A, Volkmann J, Schnitzler A, Freund HJ (1998) Detection of *n:m* Phase Locking from Noisy Data: Application to Magnetoencephalography. Physical Review Letters 81:3291-3294.

Weimann JM, Marder E, Evans B, Calabrese RL (1993) The effects of SDRNFLRFamide and TNRNFLRFamide on the motor patterns of the stomatogastric ganglion of the crab Cancer borealis. J Exp Biol 181:1-26.

Weimann JM, Skiebe P, Heinzel HG, Soto C, Kopell N, Jorge-Rivera JC, Marder E (1997) Modulation of oscillator interactions in the crab stomatogastric ganglion by crustacean cardioactive peptide. J Neurosci 17:1748-1760.

White RS, Nusbaum MP (2011) The same core rhythm generator underlies different rhythmic motor patterns. J Neurosci 31:11484-11494.

Wood DE, Stein W, Nusbaum MP (2000) Projection neurons with shared cotransmitters elicit different motor patterns from the same neural circuit. J Neurosci 20:8943-8953.

Xu H, Robertson RM (1994) Effects of temperature on properties of flight neurons in the locust. Journal of Comparative Physiology A 175:193-202.

Xu H, Meldrum Robertson R (1996) Neural parameters contributing to temperature compensation in the flight CPG of the locust, *Locusta migratoria*. Brain Research 734:213-222.

Yang F, Zheng J (2014) High temperature sensitivity is intrinsic to voltage-gated potassium channels. Elife 3:e03255.

Zečević D, Levitan H (1980) Temperature acclimation: effects on membrane physiology of an identified snail neuron. American Journal of Physiology-Cell Physiology 239:C47-C57.

Zečević D, Levitan H, Paŝić M (1985) Temperature Acclimation: Influence on Transient Outward and Inward Currents in an Identified Neurone of *Helix pomatia*. Journal of Experimental Biology 117:369.

Zheng C, Bieri KW, Hsiao YT, Colgin LL (2016) Spatial Sequence Coding Differs during Slow and Fast Gamma Rhythms in the Hippocampus. Neuron 89:398-408.